https://doi.org/10.30799/jnst.358.25100202 J. Nanosci. Tech. - Volume 10 Issue 2 (2025) 999–1005

Share Your Innovations through JACS Directory

Journal of Nanoscience and Technology

Visit Journal at https://www.jacsdirectory.com/jnst

ISSN: 2455-0191

Microwave-Assisted Z-Scheme MoO_3@TiO_2 Heterostructure Nanomaterials Emphasizing Photocatalytic Degradation of MO Dye and Antibacterial Properties

Sumaiyya Shaikh[1], Ramphal Sharma[2,*]

[1]Department of Physics, Dr. Babasaheb Ambedkar Marathwada University Aurangabad – 431 004, Maharashtra, India.
[2]Department of Physics, IIS (Deemed to be University), Jaipur – 302020, Rajasthan, India.

ARTICLE DETAILS

Article history:
Received 19 April 2025
Accepted 11 May 2025
Available online 18 May 2025

Keywords:
MoO_3
TiO_2
Z-Scheme
Antibacterial Activity
Disc Diffusion Method

ABSTRACT

An ecologically safe and efficient in terms of energy method of heterostructure photocatalysis based on metal oxide/TiO_2 and the quantity of response sites triggered by sunlight to remediate organic dye pollution have garnered a lot of interest from the research community. Two-step microwave-assisted approach has been initiated to synthesize the inexpensive, environmentally benign TiO_2 nanoparticles that adorned the MoO_3 nanocomposite. Aim of present work is to explore the photocatalytic characteristics of MoO_3@TiO_2 (MT), as well as its structural, optical, and compositional characteristics along with its bactericidal potency. By using an X-ray diffraction (XRD) instrument, the crystal structures of MT have been confirmed. PL analysis indicates MT has the lowest rate of recombination of charge carriers, implying, the charge providers have a higher lifespan and may produce more active •OH radicals during the photocatalytic process. Further, it is clear from the Reactive Oxygen Species (ROS) study that O^{2-} & OH^- are the main active species that degrade Methyl Orange (MO) dyes and play a major role in this process. MT photocatalysts were used to degrade MO dye, and the photocatalytic activity was recorded under exposure to sunlight. The MT photocatalyst shows improved degrading efficacy may be due to fast transit, strong photo-absorption, and excellent separation of the charge carriers. Additionally, the MT photocatalyst retained strong stability, low self-degradation, and great reusability after repeated cycles of the degradation process. Additionally, the improved antibacterial activities for the prepared nanocomposite were seen against gram-negative (*Escherichia coli*) and gram-positive (*Staphylococcus aureus*) bacteria analyzed by using the Disc diffusion method.

1. Introduction

The primary sources where organic contaminants are mostly found are water sources and wastewater. These pollutants are removed utilizing various chemical, physical and biological techniques, such as Oxidisation, adsorption and biological degradation (aided by microorganisms) [1, 2]. Each of these procedures has advantages and disadvantages. Photodegradation is a suitable technique for the photon-energy-based breakdown of organic pollutants. To use this approach, semiconductor photocatalysts such as TiO_2, ZnO, WO_3, Fe_2O_3, CdS, CdSe, and ZnS are needed [3,4]. The elimination of dyes and photo-induced bacterial disinfection using TiO_2 photocatalyst has been the subject of the most research out of all other oxide semiconductors [1, 5, 6, 7]. Molybdenum oxide (MoO_3), an n-type semiconductor with a narrow band gap, exhibits intriguing behaviour in terms of its chemical [8], structural [9], electrical, and optical [10] properties, making it a promising material with a broad range of stoichiometry. TiO_2 nanoparticles become significantly more hydrophilic after surface modification with MoO_3 [11, 12]. This allows them to be suspended in an aqueous solution more steadily, and it is thought that they have good dispersibility in an aqueous solution because of MoO_3's high hydrophilicity. Since TiO_2 is a semiconductor, electrons are promoted from the valence band (VB) to the conduction band (CB) upon absorption of UV radiation. A portion of the photo-formed holes in the VB recombine with the electrons in the CB, but the remaining holes, when exposed to moisture and oxygen, go through a series of intricate redox processes that produce reactive oxygen species (ROS) such as superoxide (O^{-2}). and hydroxyl radicals (-OH) [5, 13, 14]. The photocatalytic process and degradation of organic matter are carried out by these ROS. Titanium dioxide (TiO_2) is a semiconductor metal oxide with redox characteristics that can both lower the concentration of metal ions in solution and oxidize organic contaminants which makes it a strong antibacterial agent. Because of its wide bandgap TiO_2 works under the UV region to overcome, heterojunction formation with lower bandgap material is one of the dominant criteria that can work under the visible region [14].

When compared to similar bulk materials, nanoscale semiconductor clusters have notably different optoelectronic, electrical, and photocatalytic characteristics. For nanoscale materials, the primary reason for the variations is quantum size effects. The design of novel, efficient catalysts, the creation of electronic and optoelectronic devices, and photocatalysts are just a few of the many uses for these effects [5, 13, 15-17]. With these changes, the potential reactivity of photo-activated TiO_2 particles is reduced or eliminated by quenching or lowering the reactive species. When MoO_3 was added to TiO_2, the photodegradation of molasses exhibited strong activity [12, 18, 19]. Additionally, the MoO_3@TiO_2 material is more reactive under sunlight compared to the pure oxides. The altered material can absorb more light in the visible range and has a smaller band gap, which speeds up the material's breakdown [20, 21].

This study focuses on i) fabricating MoO_3@TiO_2 (MT) nanocomposite using the microwave-assisted technique, ii) investigate the produced nanocomposites' photocatalytic activity towards the methyl orange dye's degradation in the presence of solar light and iii) investigate the antimicrobial activity of the nanocomposite against *E. coli* and *S. aureus* using the disc diffusion method.

2. Experimental Methods

2.1 Sample Synthesis

2.1.1 Preparation of TiO_2 Nanoparticles

Sol-gel technique was used to synthesize TiO_2 nanoparticles. A solution of deionized water (DI) with 10 mL of isopropanol was prepared first. Next, about 20 mL of titanium tetraisopropoxide (TTIP) was added after 15 minutes into the solution. After that, the solution was hold on 80 °C with continuous stirring. Later on, the mixture cooled down to 60 °C by keeping

*Corresponding Author:sumaiyyafirdous95@gmail.com(Ramphal Sharma)

https://doi.org/10.30799/jnst.358.25100202

Cite this Article as: Sumaiyya Shaikh, Ramphal Sharma, Microwave-assisted Z-scheme MoO_3@TiO_2 heterostructure nanomaterials emphasizing photocatalytic degradation of MO dye and antibacterial properties, J. Nanosci. Tech. 10(2) (2025) 999–1005.

stirring. The solution was combined with 0.8 mL of concentrated HNO_3 and DI. After 6 hours, a dense white gel is formed and subsequently moved for heating at 300 °C for 2 hours to a furnace. The obtained TiO_2 powder was utilized in the synthesis of MT nanocomposite.

2.1.2 Synthesis of MT Nanocomposite

The experimental procedure for the preparation of MoO_3@TiO_2 (MT) heterostructure nanocomposite is illustrated in Fig. 1. Here, a microwave-assisted synthesis technique has been used to synthesize MoO_3@TiO_2 nanocatalyst. For the synthesis, materials of AR-grade quality were utilized as raw materials. As depicted in Fig. 1, in 40 mL DI water About 0.98 g of citric acid and 2.605 g ammonium hepta molybdate was added to the solution. To get a homogenous mixture of the faint blue color, solution was kept for ultrasonication for 20 minutes. After that, put on a magnetic stirrer. Within an additional beaker of 40 mL DI water, 2.54 g of thiourea was dissolved simultaneously. Subsequently combine the mixture mentioned above with the thiourea solution. pH is maintained through progressively by adding ammonia to the entire mixture, with vigorous stirring at a consistent 95 °C temperature, and pouring a mixture of (0.4 g) TiO_2 gradually. The blend was mixed until a blue-brown liquid appears. Then this mixture was transfered to a container and kept it for 15-minutes in the microwave heat (200W) treatment. Three repetitions of the microwave procedure were performed. Then, an intense dark brown precipitation was obtained; this solution was then filtered using Whatman qualitative filter paper. After keeping the dark brown suspension overnight, brown-colored powder was formed. The resultant product was first dried in the open at ambient temperature and then kept at 800 °C in a muffle furnace for two hours. Finally, gray-colored MT powder has obtained, which was further used for characterization (Fig. 1). Before the addition of TiO_2, some of the solution mixtures were collected and annealed to 600 °C for 24 hours, resulting in the whitish-gray-colored MoO_3 nanomaterial.

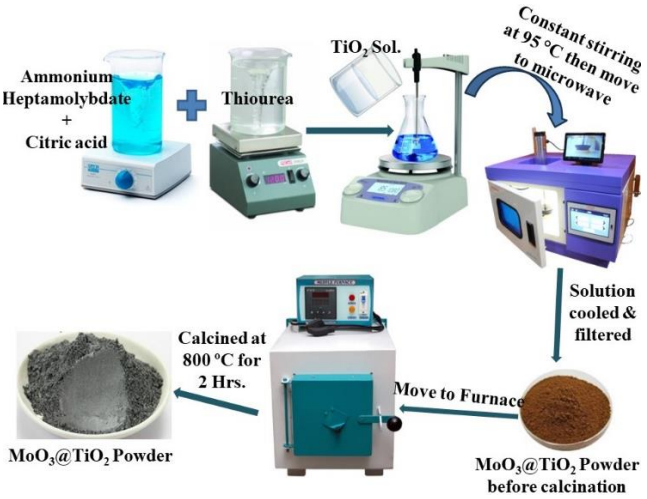

Fig. 1 Diagrammatic representation of MT synthesis using microwave technique

2.2 Experiment Setup of Methyl Orange Dye Photodegradation

Under solar irradiation, the MT heterostructure photocatalyst was measured for photocatalysis using the organic dye Methyl orange (MO), which is used as a model dye. First, a 100 mL volume beaker was filled with the MO dye aqueous solution where 10 ppm MO liquid dye was added to 100 mL of water. The weight of the synthesized nanocatalyst powder was then determined to be 0.06 g. The combined solution was continually sonicated and agitated to ensure adequate mixing and even dispersion of the photocatalysts. After that, it was stored for 25 to 30 minutes in a dark environment to reach the adsorption-desorption equilibrium. Then 5 mL of the MO dye aqueous solution was taken out after 30 minutes to record the photodegradation of the solution. The beaker with the solution was retained under the sunlight for the first reading, which was recorded at 0 minutes. Employing a UV-visible spectrophotometer, the peaks of absorption with 15-minute intervals of time were measured from these 5 mL solutions to determine the efficiency of degradation and rate-order constant of the synthesized photocatalyst. The beaker was taken out of the darkroom and placed under solar irradiation after 30 minutes.

2.3 Testing and Characterization of Materials

To analyse physical properties of as synthesized nanomaterial, at ambient temperature, X-ray diffractometer (XRD) readings (Bruker D8 Advanced) were collected providing wavelength of 0.154 nm. A step size of 0.02° was used for data measurement. Using a Perkin Elmer Lambda-25 UV-Vis spectrophotometer, Bandgap adjusting features and an optical coefficient of absorption were investigated. Using Bruker Vertex 70 spectrometer (made in Germany), the Fourier transform infrared spectroscopy (FT-IR) was used to highlight the chemical bonding in the prepared sample in the 500–4000 cm^{-1} wavelength range. The sample's surface morphological images were captured using FE-SEM (MIRA II LMH from TESCAN). Every measurement was taken at room temperature. Antibacterial activity was carried out using the disc diffusion method and the zone of inhibition was noted down.

3. Results and Discussion

3.1 Analysis of X-Ray Diffraction

To clarify the structure, x-ray diffraction (XRD) was used to characterize the synthesized sample, as shown in Fig. 2. The subsequent diffraction peaks of tetragonal TiO_2, shows the formation of polymorph, that is, rutile phase confirmed with JCPDS data card #01-076-0317. TiO_2 nanoparticles exhibited prominent peaks in diffraction for rutile phase at 27.4°, 36.0°, 41.2°, 54.3°, and 56.6° corresponds to (110), (101), (111), (211), and (220) planes respectively [22]. Peaks at 12.7°, 23.5°, 25.5°, 27.5°, 38.72°, and 57.6° assigned respectively to (020), (110), (040), (021), (060), and (171) planes revealed to orthorhombic MoO_3, accordingly JCPDS data card #01-075-0912. At last, the MT heterostructure showed peaks belonging to both orthorhombic MoO_3 and rutile TiO_2. These results, well agree with the data from conventional literatures, clearly indicate the development of MoO_3@TiO_2.

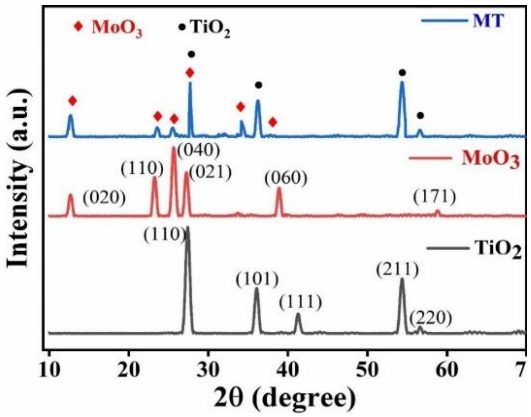

Fig. 2 X-ray diffraction graph representing TiO_2, MoO_3, and MT heterostructure nanomaterials

From the observed diffraction patterns the structural features resembling, interplanar spacing (d), lattice constant, dislocation density (δ), and crystallite size (D) are calculated [5] and tabulated in Table 1.

The Debye Scherrer's formula is given in Eq.(1),

$$D = \frac{0.94\,\lambda}{\beta cos\theta} \quad (1)$$

where, β = full-width half maxima (FWHM); λ = wavelength is 1.54056 Å.

Dislocation density (δ) was calculated by following Eq.(2),

$$\partial = \frac{1}{D^2} \quad (2)$$

As For rutile TiO_2 the lattice constants calculated as below by the Eq.(3),

$$\frac{1}{d^2} = [h^2 + k^2 + l^2(\frac{a}{c})^2]\frac{1}{a^2} \quad (3)$$

For orthogonal MoO_3, the lattice constants can be given as following Eq.(4),

$$\frac{1}{d^2} = (\frac{h}{a})^2 + (\frac{k}{b})^2 + (\frac{l}{c})^2 \quad (4)$$

Table 1 Calculated microstructural parameters of pristine TiO_2, MoO_3 and MT

Samples	Lattice constant (Å) a	c	D (nm)	∂ $(nm)^{-2}$
TiO_2	4.59	2.95	20	0.0025
MoO_3	3.92	3.66	18	0.0031
MoO_3@TiO_2 (MT)	4.32	3.29	15	0.0044

https://doi.org/10.30799/jnst.358.25100202

Cite this Article as: Sumaiyya Shaikh, Ramphal Sharma, Microwave-assisted Z-scheme MoO_3@TiO_2 heterostructure nanomaterials emphasizing photocatalytic degradation of MO dye and antibacterial properties, J. Nanosci. Tech. 10(2) (2025) 999–1005.

3.2 Surface Analysis

The typical surface electron micrographs of the TiO_2 and MT nanocomposite are illustrated in Fig. 3. As prepared TiO_2 nanoscale materials show crystals aggregate morphology as depicted in Fig. 3(a). At 200 nm resolution, illustrated in Fig. 3(b), clump formation of MT nanocomposite may result from Ostwald ripening [5], which gives rise to various nanostructures such as spheres, beads, and doughnut. Fig. 3(c) makes it easier to discern the SEM image of MT heterojunction nanocomposite on 100 nm resolution, showing beads, spheres, and a big doughnut are formed. This can be the result of the high temperature or reaction time during the composite's microwave synthesis. Supersaturation happens at higher temperatures, which speeds up the nucleation rate. This shortens the time it takes for the crystal core to grow. Nucleation replaces grain refinement as the reaction's regulatory phase. Agglomeration results from nuclear accumulation brought on by the crystal core's fast growth, which is visible at higher temperatures. The primary determinant of the ultimate product's form and texture is its rate of agglomeration [23].

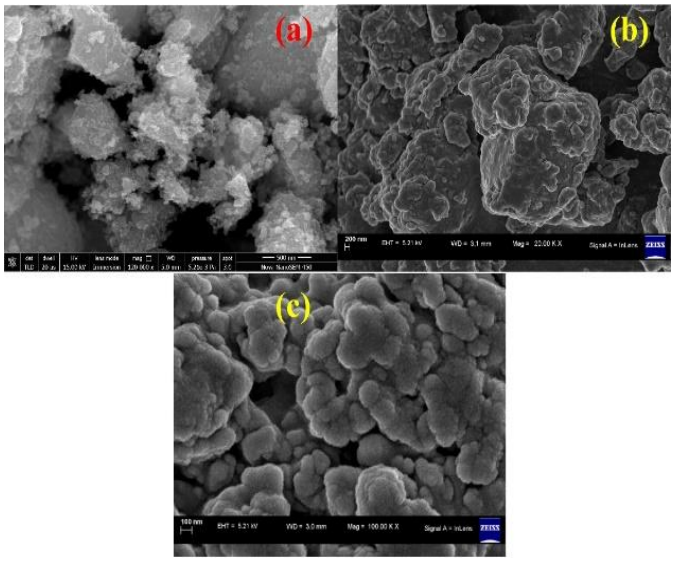

Fig. 3 FE-SEM pictures of (a) TiO2, (b) & (c) MT nanomaterials

3.3 UV-Vis Spectroscopy

To evaluate the changes in the optical bandgap that arise from comparing the responses of incident light, the UV-visible absorption spectra of MT and rutile TiO_2 were employed as depicted in Fig. 4. The graph of optical absorption shown in Fig.4(a) and the place in graph shows the bandgap Eg = 2.5 eV of the MT heterojunction photocatalyst. The MT exhibits superior absorption properties in the electromagnetic spectrum. Spectra of the absorption region for MT seem significantly red-shifted, it might be associated with the chemical bonding between MoO_3 and TiO_2. For the TiO_2 nanoparticle, the optical absorption plot is depicted in Fig. 4(b) and place in reveals the calculated bandgap Eg = 3.1 eV. The bandgap values of the MT heterojunction nanocomposite and TiO_2 were computed using Tauc's relation, which is shown in the below Eq.(5),

$$\alpha h\nu = (h\nu - Eg)^{\frac{1}{2}} \quad (5)$$

where, α = absorption coefficient, hν = photon energy, and Eg = energy bandgap of the synthesised nanomaterial.

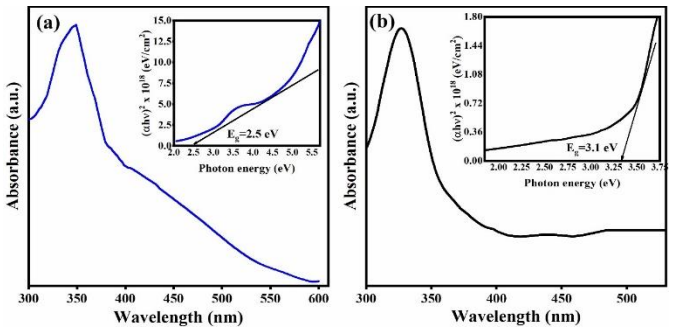

Fig. 4 Absorption spectrum with an inset of Tauc's plot of prepared photocatalyst (a) MT and (b) TiO_2 nanomaterials

Evidently, the pure TiO_2 nanoparticles' spectra exhibit a notable wavelengths less than 400 nm that are absorbed, which is related to its inherent bandgap absorption. Additionally, TM's unique heterojunction structure would enhance light harvesting. This supports their ability for photocatalysis [24].

3.4 Photoluminescence Analysis

To evaluate the photo-generated charges recombination performance PL spectra have been carried out. The PL spectra at λ_{max}=325 nm of TiO_2 and MoO_3@TiO_2 depicted in Fig. 5. The broad peak at 468 nm is the result of an electron stuck in a hole in the valance band of TiO_2 caused by an oxygen vacancy. When comparing the MoO_3@TiO_2 PL spectrum to that of TiO_2, there is a discernible peak loss at 470 nm, which accounts for its distinct heterostructure. Transmission of electrons through the photoexcited TiO_2 nanoparticle's VB to the MoO_3 CB is energetically advantageous for MoO_3@TiO_2 which inhibits the recombination of photogenerated charges. It also indicates MT has the lowest rate of recombination of charge carriers, implying, the charge providers have a higher lifespan and may produce more active •OH radicals during the photocatalytic process.

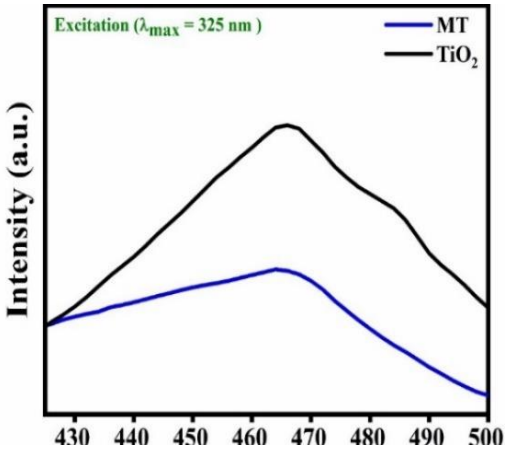

Fig. 5 PL spectra of TiO_2 and MoO_3@TiO_2 heterojunction nanocomposite

3.5 FTIR Analysis

To confirm the heterojunction structure and Ti–O–Mo bonds, FT-IR spectra of as synthesised heterojunction nanomaterial has been recorded and the results have been shown in Fig. 6. The bands at 774 and 975 cm^{-1} in the spectrum correspond to the rotation of the Ti–O–Ti bond and the vibration of the Ti–O bond, respectively [25, 26]. The characteristic band at 995 cm^{-1} indicates the molybdenum to oxygen double bond in layered orthorhombic MoO_3 phase. The Mo–O–Mo entity's bending vibrational modes are responsible for the band at 870 cm^{-1}, whereas its stretching mode vibration is attributed at 560 cm^{-1}. Lastly, it is revealed that the elongation mode of the terminal Mo–O bond is responsible for the peak at 506 cm^{-1}[26, 27]. The vibration of the Ti–O–Mo species is responsible for the appearance of an additional peak at 945 cm^{-1} in the spectra. It suggests that during the heterostructure composites' formation process, a Ti–O–Mo species forms at the point where TiO_2 and MoO_3 intersect narrowing the MoO_3@TiO_2 bandgap and enabling the flow of electrons from TiO_2 to MoO_3 under sunlight irradiation [28, 29].

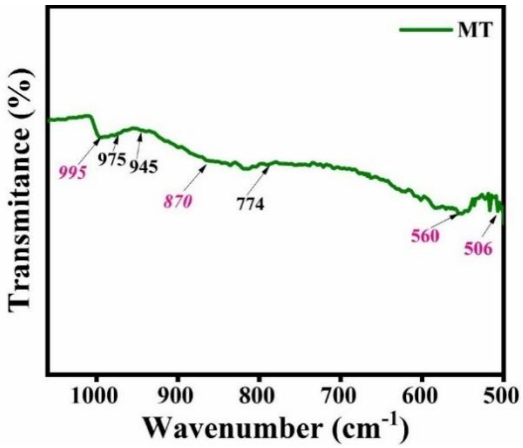

Fig. 6 FTIR Spectra of MT heterostructure nanocomposite

https://doi.org/10.30799/jnst.358.25100202

Cite this Article as: Sumaiyya Shaikh, Ramphal Sharma, Microwave-assisted Z-scheme MoO_3@TiO_2 heterostructure nanomaterials emphasizing photocatalytic degradation of MO dye and antibacterial properties, J. Nanosci. Tech. 10(2) (2025) 999–1005.

3.6 Photocatalytic Activity

In this work, the photodegradation procedure of the MT nanomaterial in sunlight conditions was investigated using the MO dye (an organic contaminant). The obtained absorbance spectra were employed to assess the activity according to the concept of rate order kinetics. The absorption measurements (Fig. 7(a)), indicates the primary peak intensity (477 nm) decline over time attribute the significant photodegradation of current nanomaterial.

At first 30 minutes, before exposure to light, the degradation was monitored in complete darkness for adsorption-desorption equilibrium. Fig. 7(b) illustrates that there is a modest decrease in comparison to photoactivity in the presence of sunlight. The photodegradation efficacy for 90 minutes was estimated Using Eq.(6),

$$\text{Photodegradation Efficiency}(\%) = \left(\frac{C_0 - C100}{C_0}\right) \times 100 \quad (6)$$

Variables affecting on the photocatalyst performance observed in sunlight are i) recombination between electron and hole pairs, ii) average crystal size and iii) absorption coefficient tuning

Furthermore, the kinetics of the degradation procedure can express as follows,

$$r = -\frac{dc}{dt} = \frac{Kks}{(1+KC)} \quad (7)$$

It can be simplified as:

$$r = -\frac{dc}{dt} = \text{kA} \quad (8)$$

It implies that the MT nanocomposite degrades the dye according to pseudo-first-order kinetics. Hence, on integrating Eq.(9), the rate constant (k) for the aforementioned nanomaterial was determined.

$$Log\left(\frac{C_0}{C_t}\right) = kt \quad (9)$$

where, C_0 stands for time t = 0 minutes, and C_t stands for time t = 90 minutes.

From the slope of the graph (Fig.7(c)), the measured value of rate constant comes out to k = 0.0219 min^{-1} for MT heterojunction nanocomposite. Compared to TiO_2 material [30], the measured k value for MT is high due to, i) the small bandgap that increases photon capacity of absorption, ii) Z-scheme heterostructure between MoO_3 & TiO_2, iii) high number of active sites and iv) microwave technique attributes modification of surface structure.

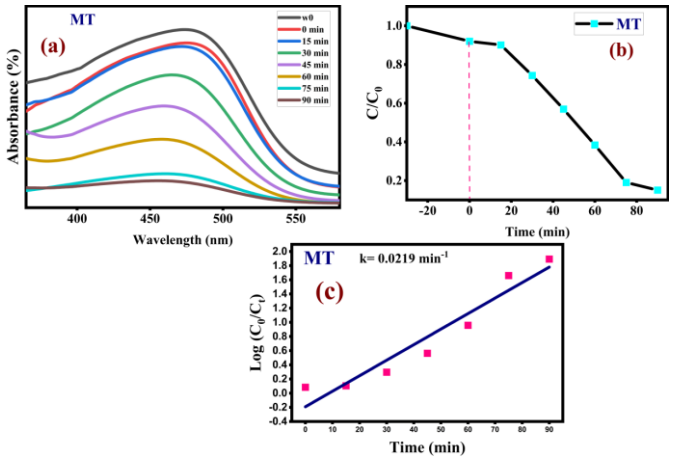

Fig.7 (a) Photodegradation spectra of respective dye with MT nanocomposite relation to time, and rate kinetics plot (b) time v/s C/C_0 and (c) time v/s log (C_0 /C_t)

3.6.1 Conceivable Mechanism Under Solar Energy for Degradation of Respective Dye using Mt Nanocomposite

An intriguing strategy for environmental protection is the water deterioration via photocatalysis contaminants accompanied by solar powered purification of water. In the current work, MT composite has been utilized for photocatalytic degradation. As seen in Fig. 8, under solar energy photons with energies greater than its band width energy (E_g), are produced by TiO_2. Since the excited charges are unstable hence, they get recombined quickly. MoO_3's Z-scheme allows it to efficiently absorb the charge carriers that photons produce, reducing the rate of recombination [31, 32]. The allocated holes can be used as an oxidant to destroy organic contaminants, while the separated electrons can be used as reluctance. Eq.(10) shows the electron-hole pairs produced during photocatalytic degradation.

$$MoO_3 / TiO_2 + h\nu = MoO_3 (h^+) / TiO_2 (e^-) \quad (10)$$

Then, the hydroxyl radicals are producing on reacting of photogenerated holes with water molecules, on the surface of the composite,

$$h^+ + H_2O \rightarrow \bullet OH + H^+ \quad (11)$$

The surface of the composite contains organic compounds which are directly oxidized by these holes and hydroxyl molecules. Produced electrons can react with atmospheric oxygen to make superoxide radical anions ($\bullet O_2^-$). Subsequently, $\bullet O^-_2$ can undergo a complex series of transformations to become •OH. consequently, the main oxidants for the degradation of MO are photoinduced holes and the hydroxyl radicals (•OH) they generate.

Initiation (Electron Attachment to Oxygen):

An electron (from radiation) combines with molecular oxygen to produce the superoxide anion radical.

$$e^- + O_2 \rightarrow \bullet O_2^-$$

Interaction with water:

Superoxide interacts with water, producing hydroperoxyl radical ($\bullet HO_2$) and hydroxide ion.

$$\bullet O_2 - + H_2O \rightarrow \bullet HO_2 + OH^-$$

Propagation:

The hydroperoxyl radical combines with water to form hydrogen peroxide (H_2O_2) and the hydroxyl radical (•OH), which is a highly reactive species.

$$\bullet HO_2 + H_2O \rightarrow H_2O_2 + \bullet OH$$

Decomposition of Hydrogen Peroxide:

Hydrogen peroxide decomposes into two hydroxyl radicals.

$$H_2O_2 \rightarrow 2\bullet OH$$

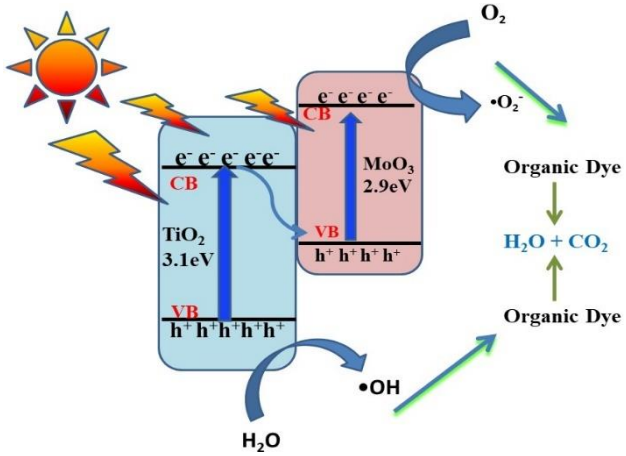

Fig. 8 Conceivable mechanism for MT heterostructure nanocomposite

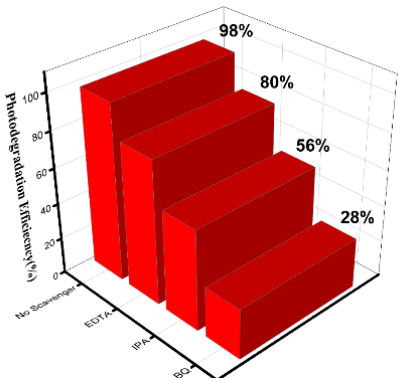

Fig. 9 The impact of several active scavengers on the prevention of MO dye degradation of nanocomposite MT

https://doi.org/10.30799/jnst.358.25100202

3.6.2 Scavenger Study

To examine the related ROS (reactive oxygen species) generated throughout the photo degradation procedure, substances that scavenge were introduced into the MO mixture. The catalyst dose was set at 0.5 g/dm^3 and the concentration was 20 mg/dm^3, with the first application occurring in the presence of sunlight. In the degradation process, Ethylenediaminetetraacetic acid disodium (Na_2EDTA/EDTA), p-benzoquinone (BQ), and isopropyl alcohol (IPA) were utilized to in order to cool the photoexcited OH, O_2^-, and holes (h^+). When p-benzoquinone (BQ) was added to the MO solution, Fig. 9 only displayed very little degradation (28%), but when IPA was present, degradation efficiency improved by 56%. When compared to BQ and IPA, EDTA exhibits approximately 80% higher degradation. This study revealed that the active species, OH and O_2^- are essential for the MO dye degradation process involving MT photocatalyst.

3.6.3 Repeatability Test

Furthermore, microwave synthesis provides a high yield of products in a shorter amount of time as compared to other conventional processes. During the analysis of MT's application in photocatalytic processes, the topic of photostability was also raised. After the first cycle photocatalyst, that was assembled kept for annealing at 80 °C then utilized in the subsequent cycles to analyze the photocatalytic cycle. After addition to the new MO dye solutions, carried out the identical steps as for the first cycle once more.

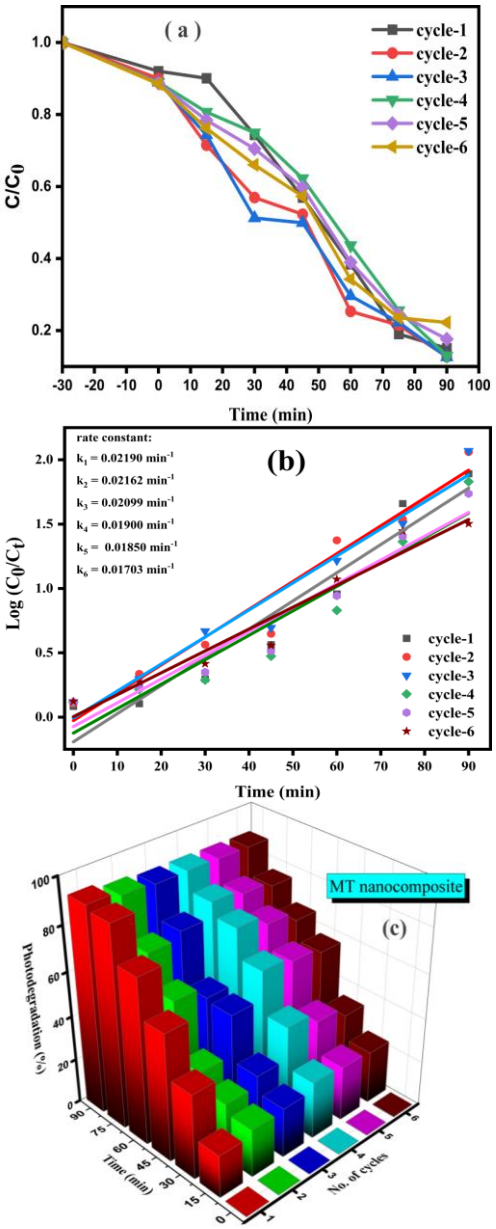

Fig. 10 Photodegradation six repeatability test cycles with heterojunction MT photocatalyst (a) photodegradation process, (b) Time vs Log (C_0/ C_t), pseudo-first-order rate constant, and (c) photodegradation efficiency for six repeated cycles

After six successive cycles, the resultant activity of photocatalysis, pseudo-first-order rate constant, and photodegradation productivity are shown in Fig. 10(a), (b), and (c), respectively. The photocatalytic activity of the MT photocatalyst is depicted in Fig. 10(a), which displays the least amount of activity aberration even after the third cycle. Nevertheless, the photocatalytic activity following the sixth cycle demonstrates improved and effective performance. Fig. 10(b) shows the pseudo-first-order rate constants that are determined for every successive cycle. When comparing the k values, there is a noticeable difference after the third cycle, and the values thereafter display minimal deviation. Fig. 10(c) illustrates the resulting photodegradation efficiency for each cycle, demonstrating a reduction in efficiency from 92% to 88.4%.

Table 2 compares the process of photocatalysis of the microwave-assisted MT nanocomposite photocatalyst with other known photocatalysts.

Table 2 Comparative data of decomposition of certain harmful dyes of different photocatalysts

S. No.	Photocatalysts	Target dye	Irradiation source	Reaction time	Degrad-ation (%)	Synthesis technique	Ref.
1.	MoO_3/Ag-TiO_2	MO	UV	5.5 hr	75.8	Sol-gel	[33]
2.	TiO_2–MoO_3	MB	Visible	4 hr	33	Electro-spinning	[34]
3.	TiO_2/MoO_3	Rhodamine B	Visible	120 min	91.4	in-situ growth method	[35]
4.	Fe_2O_3/MoO_3	MB	Visible	180 min	91.5	Microwave	[36]
5.	$ZnIn_2S_4$@MoO_3	TC-HCl	Visible	90 min	94.5	Hydrothermal	[37]
6.	MoO_3	MB	Visible	60 min	99.7	Thermal treatment	[38]
7.	MoO_3–g-C_3N_4	Mo	Solar	120 min	91	Sol-gel method	[39]
8.	MoS_2/TiO_2	MO	solar	80 min	94	Surface sensitization	[16]
9.	GO-TiO_2	MO	solar	240 min	85	Hydrothermal process	[40]
10.	TiO_2-CuO	Tetracycline	Mercury lamp	90 min	95	Microwave technique	[41]
11.	MoS_2/$BiVO_4$	TC-HCl	Visible	90 min	93.7	Microwave-assisted	[42]
12.	rGO/TiO_2	R6G	UV	240 min	80	Microwave technique	[43]
13.	N/TiO_2/rGO	Ciprofloxacin	UV	120 min	90	Microwave	[44]
14.	ZnMgS@TiO_2	MB	Visible	100 min	96.5	Coprecipita-tion method	[5]
15.	MoO_3/TiO_2	MO	Sunlight	90 min	92	Microwave-assisted	This work

3.7 Antibacterial Activity of MT

The antibacterial activity of our sample was evaluated using the agar diffusion assay (Disc diffusion method) against two bacterial strains. All three samples TiO_2, MoO_3, and MT show observable inhibition of the surrounding material determined by the zone of inhibition after a 24 h incubation period (Fig. 11). The zone of inhibition of the prepared material against gram-positive (*S. Aureus*) and gram-negative (*E. Coli*) bacteria is indicated in Table 3. Table 3 result explain that antibacterial action of all samples is superior against Gram-positive bacteria (*S. Aureus*) than Gram-negative bacteria, (*E. Coli*). This might be due to the extra outer membrane of lipopolysaccharides and peptidoglycan on the cell walls of gram-negative bacteria, which facilitates their reduction of nanoparticle resistance. [45].

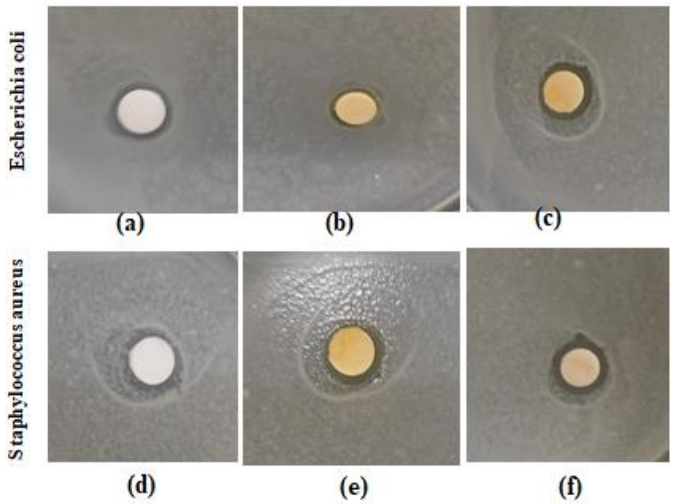

Fig. 11 Antibacterial activity against *E. coli* of (a) TiO_2, b) MoO_3 and (c) MT; *S. aureus* (d) TiO_2, (e) MoO_3 and (f) MT nanomaterials

https://doi.org/10.30799/jnst.358.25100202

Cite this Article as: Sumaiyya Shaikh, Ramphal Sharma, Microwave-assisted Z-scheme MoO_3@TiO_2 heterostructure nanomaterials emphasizing photocatalytic degradation of MO dye and antibacterial properties, J. Nanosci. Tech. 10(2) (2025) 999–1005.

Table 3 The diameter of zone inhibition of TiO_2 and MT nanomaterials

Bacteria sample	Sample code	Sample	Zone inhibition (mm)
Escherichia coli	a	TiO_2	7.14
	b	MoO_3	7.91
	c	MT	9.73
Staphylococcus aureus	d	TiO_2	7.76
	e	MoO_3	8.24
	f	MT	9.87

Furthermore, when compared to as synthesised MT nanomaterial (crystal size 15 nm), the total bactericidal potency of TiO_2 and MoO_3 nanoparticles is shown to have decreased somewhat; this could be because of their increase in crystallite size (20 and 18 nm respectively). Several study groups reported that the morphologies (particle size and shape) of distinct nanoparticles have a significant impact on their antibacterial activity [46, 47].

The antibacterial activity decreases with an increase in the crystallite size. The reason behind the size-dependent antibacterial activity of MT nanoparticles is their increased solubility in the medium as their particle size decreases. Smaller particle sizes increase solubility and cause the medium to contain more ions. This changes the pH of the medium. Ions are released and the pH changes, which causes an increase in antibacterial activity with a decrease in size. Moreover, MT photocatalyst has more bactericidal potency against the above-mentioned bacteria because of its good photocatalytic property that causes accumulation of nanoparticles inside the cell, results in reactive oxygen species (ROS) generation, causes DNA damage, or cellular protein inactivation, that may be the cause of the cell death.

The results of this study motivate us to employ MT instead of TiO_2 and MoO_3 nanoparticles as possible antimicrobial substances in a range of biological future uses in pharmaceuticals.

4. Conclusion

In this work, MoO_3@TiO_2 (MT) nanocomposite material was synthesized by using an easy, fast, and environmentally safe two-step microwave-assisted (MW) method along with sol-gel technique as a first-step. Finally, prepared samples were further utilized for the photodegradation and antibacterial applications. Before, approaching the applications, the XRD and FTIR analysis results were verified with respect to the structural and compositional studies of MT nanocomposite. The crystallite dimensions such as average crystal size of MT and TiO_2 from the XRD pattern are depicted to be 15 nm and 20 nm respectively. Optical characteristics have been evaluated; the visible region functioning of the generated nanocomposite supports MT's band gap of 2.5 eV, which is lower than TiO_2's band gap of 3.1 eV.

Furthermore, under sunlight, the photocatalytic behaviour against MO dye using the MT photocatalyst were studied and the obtained results demonstrate the improved and more effective performance of the MT photocatalyst. While observing the SEM images, agglomeration leads to the formation of different nanostructures, which may be the source of the MT nanocomposite's superior light-harvesting capacity and good photocatalytic activity. With its ability to prevent quick transferring charge and guarantee effective ion dispersion across long periods, the Z-scheme mechanism incorporating MoO_3 and TiO_2 may improve photodegradation.

Additionally, the results of the FE-SEM investigation reveals that more sites are actively operating in MT compared to TiO_2 which supports the efficient photocatalytic study of MT. PL analysis indicates MT has the lowest rate of recombination of charge carriers, implying, the charge providers have a higher lifespan and may produce more active •OH radicals during the photocatalytic process. Further, it is clear from the ROS study that O^{2-} & OH^- are the main active species that degrade MO dyes and played a major role in this process. Even after six consecutive rounds of photocatalysis, the repeatability test result supports the reusability of MT samples, and their performance is still more effective than that of other photocatalysts.

Moreover, the antibacterial activity was also studied against two bacteria, gram-positive (*S. Aureus*) and gram-negative (*E. Coli*) bacteria, bactericidal potency of the TiO_2 nanoparticles considerably enhanced their performance against *S. Aureus* and *E. Coli* on heterostructure with MoO_3 proved to be an effective antibacterial agent.

The MT nanocomposite demonstrates significant potential for the degradation of organic contaminants and various environmental pollutants under sunlight. Its visible light responsiveness and straightforward microwave-assisted synthesis process offer a cost-effective and scalable solution for environmental remediation applications.

https://doi.org/10.30799/jnst.358.25100202

Cite this Article as: Sumaiyya Shaikh, Ramphal Sharma, Microwave-assisted Z-scheme MoO_3@TiO_2 heterostructure nanomaterials emphasizing photocatalytic degradation of MO dye and antibacterial properties, J. Nanosci. Tech. 10(2) (2025) 999–1005.

Acknowledgment

The authors acknowledge Department of Physics, Dr. Babasaheb Ambedkar Marathwada University Chhatrapati Sambhaji Nagar for providing lab facilities. Sumaiyya Shaikh is thankful for the financial support from DST Inspire, New Delhi. One of the authors Prof. Ramphal Sharma is thankful to the CURIE Project (Ref. No. DST/CURIE-02/2023/IISU) funded by GOI DST New Delhi.

Disclosure Statement

The authors declare that none of their known or apparent financial conflicts could have influenced the work presented in this paper.

References

[1] K. Qi, B. Cheng, J. Yu, W. Ho, A review on TiO_2-based Z-scheme photocatalysts, Chin. J. Catal. 38 (2017) 1936-1955.
[2] N. El-Desouky, K.R. Shoueir, I. El-Mehasseb, M. El-Kemary, Bio-inspired green manufacturing of plasmonic silver nanoparticles/Degussa using Banana Waste Peduncles: Photocatalytic, antimicrobial, and cytotoxicity evaluation, J. Mater. Res. Technol. 10 (2021) 671-686.
[3] L. Fatolahi, ZnS on Cu_2Te quantum dots: preparation, characterisation, and optimisation of photocatalytic/H_2O_2 process by response surface methodology, J. Environ. Anal. Chem. 103 (2023) 1771-1785.
[4] Q. Zhou, L. Li, Z. Xin, Y. Yu, L. Wang, W. Zhang, Visible light response and heterostructure of composite CdS@ZnS–ZnO to enhance its photocatalytic activity, J. Alloys Compd. 813 (2020) 152-190.
[5] V.V. Kutwade, K.P. Gattu, F. Khan, P. Gajbar, S. Shaikh, R. Sharma, Exploration of ZnMgS loaded with biosynthesized TiO_2 as an efficient photocatalyst for solar energy mediated MB degradation, J. Mater. Sci. Mater. Electron. 34 (2023) 1133.
[6] M. Ge, Z. Hu, J. Wei, Q. He, Z. He, Recent advances in persulfate-assisted TiO_2-based photocatalysis for wastewater treatment: Performances, mechanism and perspectives, J. Alloys Compd. 888 (2021) 161625.
[7] M. Miyuchi, K. Sunada, K. Hashimoto, Antiviral Effect of Visible Light-Sensitive $CuxO/TiO_2$ Photocatalyst, J. Catal. 10 (2020) 1093.
[8] M. Jayavel, Design and fabrication of blind shoe using ATMEGA328 microcontroller and vibration motor, Int. J. Mech. Eng. 8 (2017) 1588-1593.
[9] O. Farhat, J. Faraj, F. Hachem, C. Castelain, M. Khaled, A recent review on waste heat recovery methodologies and applications: Comprehensive review, critical analysis and potential recommendations, Clean. Eng. Technol. 6 (2022) 100387.
[10] D. Meenakshi, R. Udayakumar, Protocol with hybridized Bluetooth scatternet formation for wireless network, Int. J. Appl. Eng. Res. 9 (2014) 7299-7307.
[11] T.P. Meikandaan, Experimental behavior of retrofitting of prestressed concrete Beam with FRP laminates, J. Chem. Pharm. Sci. 9 (2016) 145-148.
[12] T.P. Meikandaan, M. Hemapriya, P. Mugilvani, R. Chitra, Analysis of RC beams repaired with CFRP laminates, Int. J. Innov. Technol. Explor. Eng. 8(9S3) (2019) 768-774.
[13] V.V. Kutwade, K.P. Gattu, M.E. Sonawne, F. Kahan, D.A. Tonpe, et al., Growth and exploration of visible-light-driven enhanced photocatalytic activity of $Cu_{1-x}Cr_xS$/CdS heterojunction thin film for active dye degradation, J. Appl. Phys. A 128 (2022) 625.
[14] S. Shaikh, V.V. Kutwade, K.P. Gattu, F. Khan, P. Gajbar, et al., Formulation of microwave assisted Z-scheme MoS_2@TiO_2: explored physicochemical properties and photodegradation of MO dye, J. Dispers. Sci. Technol. (2024) 1-14.
[15] T. Di, Q. Xu, W. Ho, H. Tang, Q. Xiang, J. Yu, Review on metal sulphide-based Z-scheme photocatalysts, J. Chem. Cat. Chem. 11 (2019) 1394-1411.
[16] S.V. Kite, A.N. Kadam, D.J. Sathe, S. Patil, S.S. Mali, C.K. Hong, S.W. Lee, K.M. Garadkar, Nanostructured TiO_2 sensitized with MoS_2 nanoflowers for enhanced photodegradation efficiency toward methyl orange, J. ACS Omega 6 (2021) 17071-17085.
[17] Y. Xiaodan, W. Qingyin, J. Shicheng, G. Yihang, Nanoscale ZnS/TiO_2 composites: Preparation, characterization, and visible-light photocatalytic activity, J. Mater. Charact. 57 (2006) 333-341.
[18] N. Danyliuk, T. Tatarchuk, K. Kannan, A. Shyichuk, Optimization of TiO_2-P25 photocatalyst dose and H_2O_2 concentration for advanced photo-oxidation using smartphone-based colorimetry, J. Water Sci. Technol. 84 (2021) 469-483.
[19] J. Prakash, S. Sun, H.C. Swart, R.K. Gupta, Noble metals-TiO_2 nanocomposites: From fundamental mechanisms to photocatalysis, surface enhanced Raman scattering and antibacterial applications, J. Appl. Mater. Today. 11 (2018) 82-135.
[20] S.H. Elder, F.M. Cot, Y. Su, S.M. Heald, A.M. Tyryshkin, et al., The discovery and study of nanocrystalline TiO_2-(MoO_3) core−shell materials, J. Am. Chem. Soc. 122 (2000) 5138-5146.
[21] S. Bai, H. Liu, J. Sun, Y. Tian, S. Chen, et al., Improvement of TiO_2 photocatalytic properties under visible light by WO_3/TiO_2 and MoO_3/TiO_2 composite, J. Appl. Surf. Sci. 338 (2015) 61-68.
[22] S.B. Wategaonkar, R.P. Pawar, V.G. Parale, D.P. Nade, B.M. Sargar, R.K. Mane, Synthesis of rutile TiO_2 nanostructures by single-step hydrothermal route and its characterization, J. Mater. Today: Proc. 23 (2020) 444-451.
[23] A. Saranya, T. Devasena, H. Sivaram, R. Jayavel, Role of hexamine in ZnO morphologies at different growth temperatures with potential application in dye sensitized solar cell, J. Mat. Sci. Semicon Proc. 92 (2019) 108-115.

[24] J. Zhang, B. Li, W. Yang, Synthesis and photocatalytic performance of novel hierarchical hollow silica sphere supported TiO_2 nanoparticles, J. Mater. Sci. Lett. 117 (2014) 252-255.
[25] Y. Gao, X. Pu, D. Zhang, G. Ding, X. Shao, J. Ma, Combustion synthesis of graphene oxide–TiO_2 hybrid materials for photodegradation of methyl orange, J. Carbon 50 (2012) 4093-4101.
[26] T. López, E. Ortiz, R. Gómez, M. Picquart, Amorphous sol-gel titania modified with heteropolyacids, J. Sol-Gel Sci. Technol. 37 (2006) 189-193.
[27] T. Xia, Q. Li, X. Liu, J. Meng, X. Cao, Morphology-controllable synthesis and characterization of single-crystal molybdenum trioxide, J. Phys. Chem. B. 110 (2006) 2006-2012.
[28] M. Del Arco, S.R.G. Carrazán, C. Martín, V. Rives, J.V.G. Ramos, P. Carmona, A laser Raman spectroscopy study of molybdenum oxide supported on alumina and titania, J. Spectrochim. Acta - A: Mol. Biomol. Spectrosc. 50 (1994) 2215-2221.
[29] C. Li, Q. Xin, K.L. Wang, X. Guo, FT-IR emission spectroscopy studies of molybdenum oxide and supported molybdena on alumina, silica, zirconia, and titania, J. Appl. Spectrosc. 45 (1991) 874-882.
[30] J. He, Y. Du, Y. Bai, J. An, X. Cai, Y. Chen, P. Wang, X. Yang, Q. Feng, Facile formation of anatase/rutile TiO_2 nanocomposites with enhanced photocatalytic activity, J. Molec. 24(16) (2019) 2996.
[31] S. Li, M. Cai, Y. Liu, J. Zhang, C. Wang, et al., In situ construction of a C_3N_5 nanosheet/Bi_2WO_6 nanodot S-scheme heterojunction with enhanced structural defects for the efficient photocatalytic removal of tetracycline and Cr(VI), J. Inorg. Front. 9 (2022) 2479-2497.
[32] J. Bai, R. Shen, Z. Jiang, P. Zhang, Y. Li, X. Li, Integration of 2D layered CdS/WO_3 S-scheme heterojunctions and metallic Ti_3C_2 MXene-based Ohmic junctions for effective photocatalytic H_2 generation, Chin. J. Catal. 43 (2022) 359-369.
[33] S. Kader, M.R. Al-Mamun, M.B.K. Suhan, S.B. Shuchi, M.S. Islam, Enhanced photodegradation of methyl orange dye under UV irradiation using MoO_3 and Ag-doped TiO_2 photocatalysts, J. Environ. Technol. Innov. 27 (2022) 102476.
[34] V. Odhiambo, T.L. Ba, Z.Konya, C. Cserhati, Z. Erdelye, N.C. Naomi, I.M. Szilagyi, Preparation of TiO_2–MoO_3 composite nanofibers by water-based electrospinning process and their application in photocatalysis, J. Mater. Sci. Semicond. 147 (2022) 106699.
[35] H. Liu, T. Lv, C. Zhu, Z. Zhu, Direct bandgap narrowing of TiO_2/MoO_3 heterostructure composites for enhanced solar-driven photocatalytic activity, J. Sol. Energy Master Sol. Cells. 153 (2016) 1-8.
[36] H.T. Hsu, S.Y.Lin, Y.T. Lu, Y.Y.Chuang, S.H. Chuang, Enhanced Fenton-like process over Z-scheme MoO_3 surface decorated with Fe_2O_3 under visible light, J. Sci. Rep. 14 (2024) 8007.
[37] C. Ouyang, X. Quan, C. Zhang, S. Pan, Direct Z-scheme $ZnIn_2S_4$@MoO_3 heterojunction for efficient photodegradation of tetracycline hydrochloride under visible light irradiation, J. Chem. Eng. 424 (2021) 130510.
[38] Y. Liu, P. Feng, Z. Wang, X. Jiao, F. Akhtar, Novel fabrication and enhanced photocatalytic MB degradation of hierarchical porous monoliths of MoO_3 nanoplates, J. Sci. Rep. 7 (2017) 1845.
[39] Y. He, L. Zhang, X. Wang, Y. Wu, H. Lin, et al., Enhanced photodegradation activity of methyl orange over Z-scheme type MoO_3–g–C_3N_4 composite under visible light irradiation, J. RSC Adv. 4 (2014) 13610-13619.
[40] C. Lin, Y. Gao, J. Zhang, D. Xue, H. Fang, J. Tian, et al., GO/TiO_2 composites as a highly active photocatalyst for the degradation of methyl orange, Int. J. Mater. Res. 35 (2020) 1307-1315.
[41] A. Kubiak, Z. Bielan, M. Kubacka, E. Gabała, A.Z. Grześkowiak, et al., Microwave-assisted synthesis of a TiO_2-CuO heterojunction with enhanced photocatalytic activity against tetracycline, J. Appl. Surf. Sci. 520 (2020) 146344.
[42] C. Cheng, Q. Shi, W. Zhu, Y. Zhang, W. Su, et al., Microwave-assisted synthesis of MoS_2/$BiVO_4$ heterojunction for photocatalytic degradation of tetracycline hydrochloride, J. Nanomater. 13(9) (2023) 1522.
[43] A. Hardiansyah, W.J. Budiman, N. Yudasari, Isnaeni, T. Kida, A. Wibowo, Facile and green fabrication of microwave-assisted reduced graphene oxide/titanium dioxide nanocomposites as photocatalysts for rhodamine 6G degradation, J. ACS Omega. 6 (2021) 32166-32177.
[44] C.S. Tobon, I. Panžić, A. Bafti, G. Matijašić, D. Ljubas, L. Ćurković, Rapid microwave-assisted synthesis of N/TiO_2/rGO nanoparticles for the photocatalytic degradation of pharmaceuticals, J. Nanomater. 12(22) (2022) 3975.
[45] A.D. Russell, Similarities and differences in the responses of microorganisms to biocides, J. Antimicrob. Chemother. 52 (2003) 750-763.
[46] K.R. Raghupathi, R.T. Koodali, A.C. Manna, Size-dependent bacterial growth inhibition and mechanism of antibacterial activity of zinc oxide nanoparticles, Langmuir 27 (2011) 4020-4028.
[47] G.A. Martínez-Castañón, N.N. N. Martínez, F.M. Gutierrez, M. Mendoza, Facundo Ruiz, Synthesis and antibacterial activity of silver nanoparticles with different sizes, J. Nanoparticle Res. 10 (2008) 1343-1348.

https://doi.org/10.30799/jnst.358.25100202

Cite this Article as: Sumaiyya Shaikh, Ramphal Sharma, Microwave-assisted Z-scheme MoO_3@TiO_2 heterostructure nanomaterials emphasizing photocatalytic degradation of MO dye and antibacterial properties, J. Nanosci. Tech. 10(2) (2025) 999–1005.